Two-Dimensional Materials

Deutsche Ausgabe: DOI: 10.1002/ange.201606643
Internationale Ausgabe: DOI: 10.1002/anie.201606643

Organic-Base-Driven Intercalation and Delamination for the Production of Functionalized Titanium Carbide Nanosheets with Superior Photothermal Therapeutic Performance

Jinnan Xuan[+], Zhiqiang Wang[+], Yuyan Chen[+], Dujuan Liang, Liang Cheng, Xiaojing Yang, Zhuang Liu, Renzhi Ma, Takayoshi Sasaki, and Fengxia Geng**

Abstract: *The delamination of titanium carbide sheets, an intriguing class of two-dimensional materials, has been critically dependent on the extraction of interlayer Al in acidic media, such as concentrated hydrofluoric acid (HF) or a mixture of hydrochloric acid (HCl) and a fluoride salt. Herein, we report an organic-base-driven intercalation and delamination of titanium carbide that takes advantage of the amphoteric nature of interlayer Al. The resulting aluminum-oxoanion-functionalized titanium carbide sheets manifested unusually strong optical absorption in the near-infrared (NIR) region with a mass extinction coefficient as high as 29.1 $L g^{-1} cm^{-1}$ at 808 nm. Thus, the performance of this material is comparable or even superior to that of state-of-the-art photoabsorption materials, including gold-based nanostructures, carbon-based materials, and transition-metal dichalcogenides. Preliminary studies show that the titanium carbide sheets serve as efficient photothermal agents against tumor cells.*

Photothermal therapy (PTT), a therapeutic strategy in which photon energy is converted into heat to destroy tumor cells through hyperthermia, is a potential substitute treatment approach for conventional clinical cancer therapies, such as surgery, radiotherapy, and chemotherapy.[1,2] In addition to well-studied photoabsorbers, such as noble-metal nanoparticles,[3] nanoshells,[4] nanorods,[5] and carbon nanotubes,[6] two-dimensional (2D) nanosheets have emerged as an important family of potentially pertinent photoabsorber candidates because of an exceptional surface-area-to-mass ratio and high cargo loadings, as demonstrated in vitro and in vivo in several studies on graphene oxide (GO),[7] reduced graphene oxide (rGO),[8] MoS_2,[9] and MnO_2 sheets.[10] However, although a variety of 2D nanosheets have been created, including well-known graphene, sheets of clays, hexagonal boron nitrides (*h*-BNs),[11] transition-metal chalcogenides (TMCs),[12] and metal oxides and hydroxides,[13] only a few of these materials meet the prerequisite of enhanced absorption in the biological NIR region, and the development of novel 2D sheets that are suitable for use in cancer photothermal ablation therapy is becoming increasingly desirable but is highly challenging.

In this study, we targeted a newly discovered sheet catalogue, the early-transition-metal carbides referred to as MXenes, for use as novel phototherapeutic agents. MXenes are chemically delaminated from $M_{n+1}AX_n$ or MAX phases, in which M denotes an early transition metal, A represents an element of Group 13 or 14, and X is C and/or N.[14] MAX phases characteristically show a structure consisting of stacked $M_{n+1}X_n$ layers with neighboring layers "glued" with A atoms. This arrangement results in structural anisotropy with strong in-plane M–X bonds featuring metallic, covalent, and ionic bonding, whereas the interplanar M–A metallic bonds are relatively weak.[15] The isolation of elementary MXenes from the stacked structure relies critically on artificial cleavage of the relatively weak M–A bonds through the selective extraction of the A layer. This process is accompanied by the mediation of surface transition metals with anions in the solution environment, for example, OH^- and/or F^- in the case of reactions occurring in aqueous HF. In this way, the metallic M–A bonds are replaced with weaker hydrogen bonds, thus easing the further intercalation of organic guests, such as dimethyl sulfoxide, urea, H_2O, and consequently resulting in final delamination into single units under an external shearing force.[16]

Herein, on the basis of the most widely studied Ti_3AlC_2 as an illustrating example, we report a completely different method to produce 2D functionalized titanium carbide (hereafter referred to as TC) sheets with strong NIR absorbance. We show that these nanosheets are suitable for application in photothermal therapy. In contrast to conventional wisdom on the production of TC sheets, for which acidic media, such as strongly corrosive concentrated HF or a mixture of HCl and a fluoride salt, have typically been used to selectively extract

[*] J. N. Xuan,[+] Z. Q. Wang,[+] F. X. Geng
College of Chemistry, Chemical Engineering and Materials Science
Soochow University
Suzhou 215123 (China)
E-mail: gengfx@suda.edu.cn
Y. Y. Chen,[+] L. Cheng, Z. Liu
Institute of Functional Nano and Soft Materials (FUNSOM)
Soochow University
Suzhou 215123 (China)
E-mail: lcheng2@suda.edu.cn
D. J. Liang, X. J. Yang
College of Chemistry, Beijing Normal University
Beijing 100875 (China)
R. Z. Ma, T. Sasaki
International Center for Materials Nanoarchitectonics
National Institute for Materials Science
1-1 Namiki, Tsukuba, Ibaraki 305-0044 (Japan)
[+] These authors contributed equally.
Supporting information and the ORCID identification number(s) for the author(s) of this article can be found under http://dx.doi.org/10.1002/anie.201606643.

the Al layer, in this study we employed an organic base, tetramethylammonium hydroxide (TMAOH), as the etchant, in view of the amphoteric nature of Al, which therefore reacts with both acids and bases. TMAOH was selected for two reasons. First, TMAOH is very efficient in attacking Al, which is the main reason that it has been widely used as a major ingredient of commercial developers for Al etching. Second, the $Al(OH)_4^-$ formed in the reaction of Al with TMAOH can readily serve as a titanium-mediation moiety on the TC layer surface. Additionally, the cleavage of the Ti–Al bond enables the bulky TMA^+ cation to access the gallery space, thereby facilitating delamination. Importantly, modification of the TC sheet surface by the Al oxoanions imparts the sheets with strong and broad absorption in the NIR region, thereby resulting in excellent phototherapeutic behavior for the targeting of tumor cells. A schematic illustration showing the intercalation and delamination of the Ti_3AlC_2 structure is provided in Figure 1.

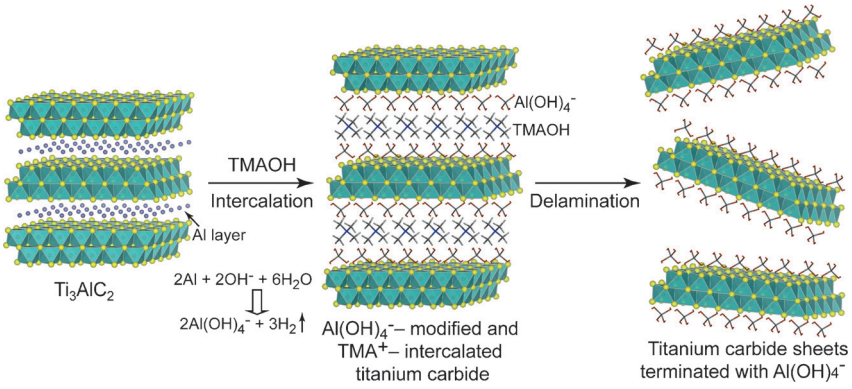

Figure 1. Schematic illustration showing the intercalation and delamination process. The organic base, TMAOH, reacts with the Al atomic layer in the gallery to promote key processes, including cleavage of the Ti–Al bonds through Al hydrolysis, modification of the TC unit surface with $Al(OH)_4^-$, and the intercalation of bulky TMA^+ into the gallery, in a single step. The cleavage of Ti–Al metallic bonds and bulky-ion intercalation facilitates the subsequent disassembly of the precursor layered crystals into their elementary layers.

When the as-received crystals came in contact with the TMAOH solution, bubbles immediately formed (see the Supporting Information). This effervescence indicated an efficient chemical reaction with the bases. The bubbles were inferred to be due to the liberation of H_2 gas according to the reaction $2Al + 2OH^- + 6H_2O \rightarrow 2[Al(OH)_4]^- + 3H_2$. As the Ti_3AlC_2 surface had a very high tendency to be passivated by a thin oxidation layer, pretreatment in very dilute HF for the removal of the passivation layer was necessary to improve the efficiency (see Supporting Information). The sample structure was characterized by X-ray diffraction (XRD; Figure 2a). The as-received powder was identified as pure-phase Ti_3AlC_2 with most of the reflections well-incorporated in a two-layer 2H polytype with hexagonal symmetry (space group: $P6_3/mmc$). The unit-cell values were refined as $a = 0.307138(8)$ nm and $c = 1.853983(1)$ nm. The basal spacing between the layers corresponded to $c/2$, 0.92 nm, which was roughly consistent with the sum of the unilamellar sheet thickness of 0.75 nm and the size of an aluminum atom (0.13 nm). The crystallites were in a typical platelike morphology for layered materials with a lateral dimension of 5–10 μm and a thickness of hundreds of nanometers (see the Supporting Information). After cleaning of the oxidation surface, the reaction in the TMAOH solution for even a short period of 5 min resulted in the occurrence of a new peak corresponding to an expanded layer spacing of 1.50 nm (see the Supporting Information) and indicating the successful intercalation of TMA ions. When the reaction time with TMAOH was extended to 24 h, the intensity of the 1.50 nm peak became dominant, whereas that of the original peak with a d spacing of 0.92 nm shrank to a negligible value, thus implying nearly complete phase conversion. The diffraction peaks were well-defined with full-width at a half-maximum (FWHM) as narrow as 0.614°, which indicated that the intercalation was almost uniform and the intercalated sample was well-crystallized. Notably, only the basal reflections $00l$ with $l = 2n$ (n equaling the odd numbers) 002, 006, and 0010 were apparent, whereas 004 and 008 were quite weak and could be observed only when enlarged. To determine the origin of the weakening of the intensities of 004 and 008, the basal reflections for the unit layers stacked with an enlarged spacing of 1.5 nm were numerically simulated (see the Supporting Information for details). It was obvious that 004 and 008 were only of negligible intensity, in contrast with the strong 002, 006, and 0010 diffractions, in good agreement with the experimental observations.

We used X-ray photoelectron spectroscopy (XPS) to gain more information on the reaction and surface functionalities. In the original Ti_3AlC_2 powder, signals corresponding to the element O, fitted to O–Ti and O–Al, were detected in addition to those for Ti, Al, and C. This result, combined with the observation of a concentrated spatial distribution at the crystal edges in O elemental mapping (see the Supporting Information), confirmed the existence of an oxidation passivation layer on the outer crystal surface. After the reaction in aqueous TMAOH, the sample exhibited an additional signal for N at approximately 400 eV, thus confirming the intercalation of the TMA ions. Notably, no significant Al loss was found, with the Al/Ti atomic ratio determined by inductively coupled plasma (ICP) analysis to be 0.89 : 3, which was similar to the original value of 1:3.

We believed the reaction mechanism in the present study to be totally different to that of Al deintercalation conducted in concentrated HF, in which Al loss was quite severe with an Al/Ti ratio below 0.1:3.[15,17] It is known that the reaction of Al with TMAOH hydrolyzes Al to yield $Al(OH)_4^-$. Owing to its negative charge, $Al(OH)_4^-$ would be immediately susceptible to bonding with the surface Ti metals of the unit layer through O–Ti bonds, thus resulting in a structure with Ti_3C_2 sheets terminated by $Al(OH)_4^-$ and sandwiching TMA^+ (Figure 2b). In such a configuration, one Al atom would be replaced with

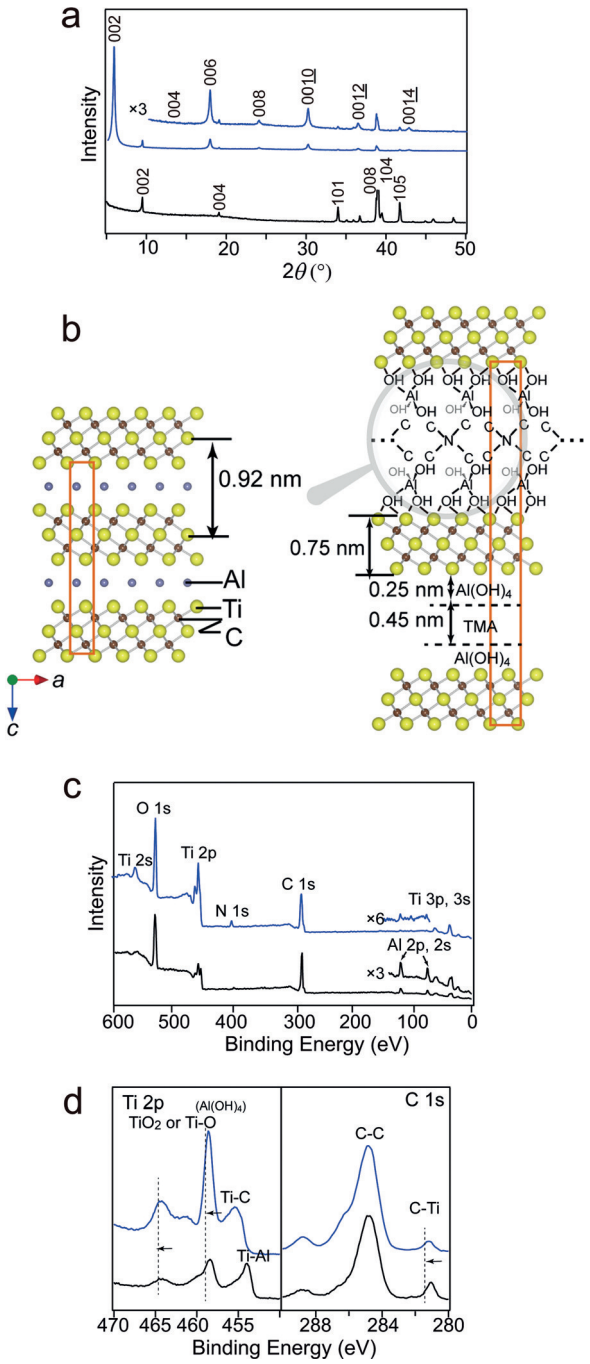

Figure 2. Structural characterization of the sample after TMA intercalation as compared with original Ti_3AlC_2. a) XRD profiles of the samples before and after reaction in aqueous TMAOH, showing an expansion of the basal spacing from 0.92 to 1.50 nm. b) Structural illustration of Ti_3AlC_2 before and after the reaction with TMAOH.[21] c) XPS survey and d) high-resolution spectra for the Ti 2p and C 1s regions.

one $Al(OH)_4^-$ moiety, which may be responsible for the little loss of Al in the reaction with aqueous TMAOH.

Fitting analysis of the O 1s XPS spectrum showed the presence of fractions of O–Ti, O–Al, and –OH, thus corroborating the inclusion of $Al(OH)_4^-$ and its bonding with Ti on the sheet surface. Additionally, it was previously reported that OH^- and F^- mediation in the substitution of gallery Al atoms may withdraw valence electrons from Ti atoms and subsequently from C atoms, thus normally resulting in a shift to higher energies for Ti–O and carbide species,[18] as indicated by the dashed lines and arrows in Figure 2d. However, the present TC sample terminated with $Al(OH)_4^-$ did not exhibit such a shift, possibly owing to additional electron injection and balance from Al through Al–O bonding. All these results verified the structural model, in which TC sheet units were terminated by $Al(OH)_4^-$ through the bonding of O atoms of $Al(OH)_4^-$ to surface Ti atoms of Ti_3C_2 sheets, and TMA^+ was in the gallery connecting the sheets through electrostatic forces. Zooming in on the sheet structure, $Al(OH)_4^-$ ions with a tetrahedral geometry may stack on both sides of Ti_3C_2 sheets with an atom sequence of –Ti–O–Al–O–. Interestingly, the O–O distance in $Al(OH)_4^-$ tetrahedra almost matched the Ti–Ti distance of approximately 0.3 nm in the closely packed Ti layers, from which it is reasonable to suppose that the O layer bonded with surface Ti atoms was also in a close-packed geometry. Additionally, previous density functional theory (DFT) studies on the configuration of OH^- connected to Ti suggested that closely packed O atoms located at the sites above Ti(2) atoms are most structurally stable,[14,19] which should also be applicable to the first O layer of $Al(OH)_4^-$. From the viewpoint of crystal chemistry, neighboring ions may share O–H bonding, thus forming a linked close-packed planar network for both Al and O layers. Only half of the positions in the Al layer could be occupied, considering that only one Al atom was available to two surface Ti atoms, for which configuration the nominal composition would be $Al_{0.5}(OH)_2$, in good agreement with the experimental formula of $Al(OH)_4$.[20]

Owing to the successful intercalation of bulky TMA ions, even gentle shaking by hand or repeated washing of the TMA-intercalated phase resulted in significant delamination and readily produced a colloidal suspension of TC nanosheets. The dispersion was centrifuged at 3500 rpm to remove the unreacted powder. Separation of the supernatant yielded a black liquid (Figure 3a). The concentration, C, of the as-obtained dispersion was measured by filtration and weighing and was determined to be 1.05 gL^{-1}. Tyndall light scattering of laser light directed through the suspension was clearly observed as a result of the dispersion of TC nanosheet crystallites in the aqueous suspension. ICP analysis of the so-obtained colloidal suspension gave an Al/Ti ratio of 0.83:3, which does not deviate much from the value for the stacked phase after Al hydrolysis and TMA^+ intercalation (see

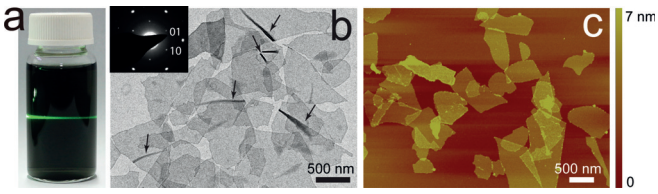

Figure 3. Characterization of the as-obtained TC nanosheets. a) Photograph of the nanosheet dispersion in H_2O showing an apparent Tyndall effect. b) Representative bright-field TEM and c) AFM image of the extremely thin delaminated nanosheets. Inset in (b): SAED pattern.

above), thus implying that $Al(OH)_4^-$ remained bonded to TC sheets. The negative ξ potential of the sheet colloid, measured to be −22.0 mV, provided further evidence that the surfaces of the TC sheets were negatively charged.

The structure of the obtained TC sheets was studied by transmission electron microscopy (TEM), which revealed a two-dimensional structure with lateral dimensions in the range of 500–1000 nm (Figure 3b). The sheet was almost transparent, thus indicating a high degree of delamination into extremely thin sheets. In some places, the sheets were crumpled or scrolled, as marked with arrows, which suggested that the sheets were highly flexible. The corresponding selected-area electron diffraction (SAED) pattern shown in the inset of Figure 3b showed a spot pattern, which confirmed that the sheet was single-crystalline. All the diffraction spots could be indexed as *hk* reflections of a hexagonal lattice with $a = 0.31$ nm, thus suggesting that the hexagonal structure of the basal planes remained intact during the disassembly process.

Atomic force microscopy (AFM) provided further evidence for the formation of thin nanosheets (Figure 3c). The clear observation of edges, even for the underlying sheets, confirmed their ultrathin character. By line scanning across the plain area of the sheet, the height was estimated to be approximately 1.6–2.0 nm, thus providing evidence that the substance in the colloidal solution indeed consisted of monolayer or bilayer sheets. The crystallographic thickness of the TC sheets was calculated to be 0.75 nm on the basis of their atomic architecture, and the difference between this value and that obtained from AFM characterization was probably associated with the capping of the Al oxoanions (0.5 nm = 0.25 nm × 2) and the occasionally unavoidable attachment of counter TMA^+ ions (0.45 nm) to the sheet surfaces. With $Al(OH)_4^-$ terminating the surfaces, the sheets were of relatively high stability, and no significant degradation was found except in a strongly oxidizing environment. Interestingly, the degradation typically followed a two-step oxidation process, that is, passivation of $Al(OH)_4^-$ and oxidation of Ti_3C_2 to TiO_2 (see the Supporting Information for details), thus providing further evidence that $Al(OH)_4^-$ played an important role in stabilizing the TC sheets.

Owing to mediation by the Al oxoanions $Al(OH)_4^-$ on the sheet surface, a colloidal suspension of the TC sheets showed enhanced NIR absorbance and a broad absorption from 560 to 1200 nm with a maximum at approximately 800 nm. This maximum fell in the first NIR window (750–900 nm) and perfectly matched the wavelength of most commonly used lasers in practical applications. The presence of surface functional groups has been demonstrated to dramatically alter the properties of titanium carbide nanosheets.[15] For example, OH^-- and/or F^--functionalized derivatives were nonmagnetic narrow-band-gap semiconductors or metals, whereas pristine Ti_2C and Ti_3C_2 layers with a clean surface were predicted and experimentally proven to behave as magnetic metals.[22] When the TC sheets were produced by completely extracting the Al layer with concentrated HF, in which case the sheets were terminated with OH^- or F^-, only negligible absorption enhancement in the NIR region was detected (see the Supporting Information), thus further confirming that surface termination by the Al oxoanion played an important role in NIR absorption. As the observed NIR absorption was very broad, it might be due to the localized surface plasmon resonance (LSPR) effect; an in-depth study to elucidate the exact mechanism is under way. The optical absorbance scaled linearly with concentration, thus suggesting that the sheets were completely delaminated and there was no association between the sheets in this concentration range. The strong absorption in the NIR region suggested the potential of the sheets as excellent photothermal agents. The mass extinction coefficient at 808 nm, a gauge for evaluating the efficiency of light absorption, was calculated according to the Lambert-Beer law to be 29.1 $L\,g^{-1}\,cm^{-1}$, which is comparable to or even higher than those of most documented photoabsorption materials (Figure 4a), for example, 13.9 for Au nanorods,[23] 23.8 for WS_2 nanosheets,[24] 29.2 for MoS_2 nanosheets,[9b] 3.6 for graphene oxide (GO),[23] 24.6 for reduced GO,[23] and 14.8 for black phosphorus[25] (see the Supporting Information for a more detailed comparison of the mass extinction coefficient of the TC sheets in this study with those of other reported materials).

The strong and broad absorption in the NIR region motivated us to assess the possibility of using TC sheets as a new photothermal agent for anticancer therapy. To this end, we first studied the photothermal conversion behavior of the sheets. Poly(ethylene glycol) (PEG) was used to modify the as-synthesized TC sheets. The resulting material exhibited excellent stability in various physiological solutions. Figure 4b shows the temperature elevation of the sheet colloid when subjected to 808 nm laser irradiation at differing power densities. At 0.8 $W\,cm^{-2}$, irradiation for 5 min increased the colloid temperature above the photoablation limit of 60 °C. In comparison, under the same irradiation conditions, no apparent temperature increase was observed for pure H_2O, which retained an almost steady temperature of 23.5 °C, and the temperature for TC sheets terminated with OH^- and/or F^- was limited below 50 °C (see the Supporting Information), thus suggesting that the as-obtained TC nanosheets with Al oxoanion termination did exhibit an enhanced photothermal effect. Furthermore, the photostability of the TC sheets was compared with that of Au nanorods and indocyanine green (ICG), which are the two nanomaterials most widely used as light absorbers in laser-mediated PTT, by repeating 5 cycles of photoablation of 3 min each. The results showed that the photostability of the TC nanosheets was superior to that of Au nanorods and ICG (see the Supporting Information).

Motivated by the excellent photothermal properties of the TC sheets, we continued to test their efficacy for in vitro photothermal cancer therapy. The standard methyl thiazolyl tetrazolium (MTT) assay was first carried out to determine the relative viabilities of 4T1 murine breast cancer cells. After cells were incubated with TC sheets at various concentrations for 24 h, no significant cytotoxicity of the TC sheets was observed even at high concentrations up to 50 $\mu g\,mL^{-1}$ (Figure 4c). Next, we used TC sheets as a photothermal agent for in vitro cancer-cell ablation under laser irradiation. 4T1 cells containing TC sheets were irradiated with an 808 nm laser at power densities of 0, 0.1, 0.2, 0.4, 0.6, 0.8, and

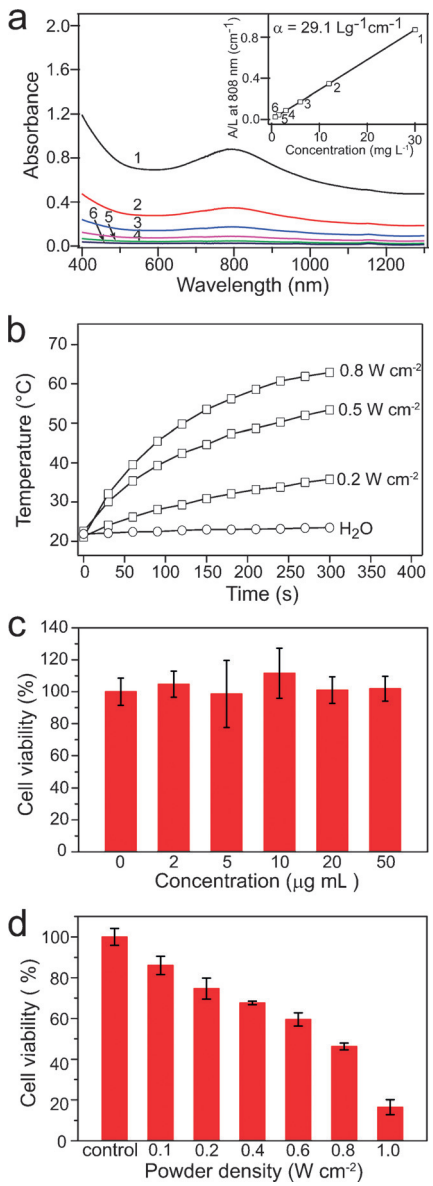

Figure 4. In vitro photothermal cancer therapy. a) NIR absorption spectra for the colloidal sheet suspensions. Inset: Beer law absorbance plot for absorption at 808 nm. b) Photothermal heating curves of TC nanosheets at various power densities. c) Relative viability of 4T1 cells after incubation with TC sheets at various concentrations. d) Relative viability of 4T1 cells after photothermal ablation induced by TC sheets at different power densities. The concentration of TC sheets was 50 μg mL^{-1}.

1.0 W cm^{-2} for 5 min (Figure 4d). Upon irradiation, the 4T1 cells were found to exhibit a drastic decline in viability with increasing laser power density. The in vivo laser treatment of tumor-bearing mice injected with the $Al(OH)_4^-$-functionalized TC sheets also showed an efficient and rapid heating effect (see the Supporting Information). Taken together, these observations demonstrated that the aluminum-oxoanion-terminated TC sheets described herein could potentially serve as excellent photothermal therapeutic agents. The infinite choice of MAX phases will enable further diversification of the sheet composition and provide enormous possibilities for optimizing their performance. Furthermore, the facile and rich surface chemistry of this class of materials promises the simultaneous delivery of drugs, ligands, or imaging contrast agents, thus opening avenues for the future design of multifunctional theranostic nanoplatforms.

In summary, we have reported that the reaction of gallery Al with an organic base, TMAOH, produces monolayer or bilayer TC sheets surface-functionalized with hydrolyzed $Al(OH)_4^-$ that possess an unusually enhanced ability to absorb light in the NIR region. Our study shows the opportunities offered by the novel material, which functions as a very efficient photothermal agent. The mass extinction coefficient is as high as 29.1 L g^{-1} cm^{-1} at 808 nm, which is comparable to and even higher than those of state-of-the-art NIR-absorption materials, such as gold-based nanostructures, carbon-based materials, and transition-metal dichalcogenides. This study demonstrates a new pathway for disassembling layered materials and also opens up new aveneus for developing MAX phases with desirable properties for a wealth of applications.

Acknowledgements

We acknowledge financial support from the National Natural Science Foundation of China (51402204 and 51572180), the Thousand Young Talents Program, the Jiangsu Specially Appointed Professor Program, and a project funded by Priority Academic Program Development (PAPD) of Jiangsu Higher Education Institutions.

Keywords: delamination · layered structures · materials science · photothermal therapy · titanium carbide

How to cite: *Angew. Chem. Int. Ed.* **2016**, *55*, 14569–14574
Angew. Chem. **2016**, *128*, 14789–14794

[1] a) W. I. Choi, J.-Y. Kim, C. Kang, C. C. Byeon, Y. H. Kim, G. Tae, *ACS Nano* **2011**, *5*, 1995; b) L. Cheng, C. Wang, L. Feng, K. Yang, Z. Liu, *Chem. Rev.* **2014**, *114*, 10869.
[2] Y. Liu, K. Ai, L. Lu, *Chem. Rev.* **2014**, *114*, 5057.
[3] Z. Qin, J. C. Bischof, *Chem. Soc. Rev.* **2012**, *41*, 1191.
[4] R. Bardhan, S. Lal, A. Joshi, N. J. Halas, *Acc. Chem. Res.* **2011**, *44*, 936.
[5] X. Huang, I. H. El-Sayed, W. Qian, M. A. El-Sayed, *J. Am. Chem. Soc.* **2006**, *128*, 2115.
[6] N. W. S. Kam, M. O'Connell, J. A. Wisdom, H. Dai, *Proc. Natl. Acad. Sci. USA* **2005**, *102*, 11600.
[7] W. Zhang, Z. Guo, D. Huang, Z. Liu, X. Guo, H. Zhong, *Biomaterials* **2011**, *32*, 8555.
[8] K. Yang, S. Zhang, G. Zhang, X. Sun, S.-T. Lee, Z. Liu, *Nano Lett.* **2010**, *10*, 3318.
[9] a) T. Liu, C. Wang, X. Gu, H. Gong, L. Cheng, X. Shi, L. Feng, B. Sun, Z. Liu, *Adv. Mater.* **2014**, *26*, 3433; b) S. S. Chou, B. Kaehr, J. Kim, B. M. Foley, M. De, P. E. Hopkins, J. Huang, C. J. Brinker, V. P. Dravid, *Angew. Chem. Int. Ed.* **2013**, *52*, 4160; *Angew. Chem.* **2013**, *125*, 4254.
[10] Y. Chen, D. Ye, M. Wu, H. Chen, L. Zhang, J. Shi, L. Wang, *Adv. Mater.* **2014**, *26*, 7019.
[11] N. I. Kovtyukhova, Y. Wang, A. Berkdemir, R. Cruz-Silva, M. Terrones, V. H. Crespi, T. E. Mallouk, *Nat. Chem.* **2014**, *6*, 957.
[12] A. O'Neill, U. Khan, J. N. Coleman, *Chem. Mater.* **2012**, *24*, 2414.

[13] a) R. Ma, T. Sasaki, *Acc. Chem. Res.* **2015**, *48*, 136; b) R. E. Schaak, T. E. Mallouk, *Chem. Mater.* **2000**, *12*, 3427.
[14] M. Naguib, M. Kurtoglu, V. Presser, J. Lu, J. Niu, M. Heon, L. Hultman, Y. Gogotsi, M. W. Barsoum, *Adv. Mater.* **2011**, *23*, 4248.
[15] a) M. Naguib, V. N. Mochalin, M. W. Barsoum, Y. Gogotsi, *Adv. Mater.* **2014**, *26*, 992; b) M. Naguib, Y. Gogotsi, *Acc. Chem. Res.* **2015**, *48*, 128.
[16] a) O. Mashtalir, M. Naguib, V. N. Mochalin, Y. Dall'Agnese, M. Heon, M. W. Barsoum, Y. Gogotsi, *Nat. Commun.* **2013**, *4*, 1716; b) M. Ghidiu, M. R. Lukatskaya, M.-Q. Zhao, Y. Gogotsi, M. W. Barsoum, *Nature* **2014**, *516*, 78.
[17] M. Naguib, J. Halim, J. Lu, K. M. Cook, L. Hultman, Y. Gogotsi, M. W. Barsoum, *J. Am. Chem. Soc.* **2013**, *135*, 15966.
[18] J. Halim, M. R. Lukatskaya, K. M. Cook, J. Lu, C. R. Smith, L.-Å. Näslund, S. J. May, L. Hultman, Y. Gogotsi, P. Eklund, M. W. Barsoum, *Chem. Mater.* **2014**, *26*, 2374.
[19] Q. Tang, Z. Zhou, P. Shen, *J. Am. Chem. Soc.* **2012**, *134*, 16909.
[20] The structure proposed is close to that of a natural mineral, gibbsite (γ-$Al(OH)_3$), in which two planes of O atoms in a hexagonal network are layered around a plane of Al atoms in which only 2/3 of the Al positions are occupied.
[21] In the structural model with $Al(OH)_4^-$ capping the unit layer and TMA^+ intercalated between layers, the basal spacing should be 1.7 nm. The experimentally observed value of 1.5 nm is thought to result from partial or complete dehydration of $Al(OH)_4^-$.
[22] a) C. Xu, L. Wang, Z. Liu, L. Chen, J. Guo, N. Kang, X.-L. Ma, H.-M. Cheng, W. Ren, *Nat. Mater.* **2015**, *14*, 1135; b) A. N. Enyashin, A. L. Ivanovskii, *J. Phys. Chem. C* **2013**, *117*, 13637.
[23] J. T. Robinson, S. M. Tabakman, Y. Liang, H. Wang, H. Sanchez Casalongue, D. Vinh, H. Dai, *J. Am. Chem. Soc.* **2011**, *133*, 6825.
[24] L. Cheng, J. Liu, X. Gu, H. Gong, X. Shi, T. Liu, C. Wang, X. Wang, G. Liu, H. Xing, W. Bu, B. Sun, Z. Liu, *Adv. Mater.* **2014**, *26*, 1886.
[25] Z. Sun, H. Xie, S. Tang, X.-F. Yu, Z. Guo, J. Shao, H. Zhang, H. Huang, H. Wang, P. K. Chu, *Angew. Chem. Int. Ed.* **2015**, *54*, 11526; *Angew. Chem.* **2015**, *127*, 11688.

Received: July 8, 2016
Revised: September 5, 2016
Published online: October 24, 2016

